RSC Advances

This article can be cited before page numbers have been issued, to do this please use: G. Kandasamy, S. Surendran, A. Chakrabarty, S.N. Kale and D. Maity, *RSC Adv.*, 2016, DOI: 10.1039/C6RA18567C.

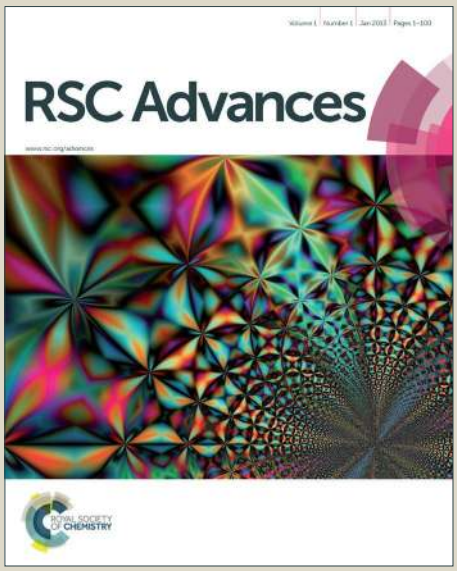

ROYAL SOCIETY OF CHEMISTRY

www.rsc.org/advances

View Article Online
DOI: 10.1039/C6RA18567C

FACILE SYNTHESIS OF NOVEL HYDROPHILIC AND CARBOXYL-AMINE FUNCTIONALIZED SUPERPARAMAGNETIC IRON OXIDE NANOPARTICLES FOR BIOMEDICAL APPLICATIONS

Ganeshlenin Kandasamy [1], Sreeraj Surendran [2], Anindita Chakrabarty [2], S. N. Kale [3], Dipak Maity [1]*

[1]*Department of Mechanical Engineering, Shiv Nadar University, Uttar Pradesh 201314, India*

[2]*Department of Life sciences, Shiv Nadar University, Uttar Pradesh 201314, India*

[3]*Department of Applied Physics, Defence Institute of Advanced Technology, Pune 411025, India*

* Corresponding author: dipak.maity@snu.edu.in

ABSTRACT:

In this work, we aim to synthesize water soluble and surface functionalized superparamagnetic iron oxide nanoparticles (SPIONs) using novel surfactants such as terephthalic acid (TA), 2-aminoterephthalic acid (ATA), trimesic acid (TMA) and pyromelltic acid (PMA) through one-step facile chemical co-precipitation and thermal decomposition methods. The as-synthesized SPIONs are characterized using X-ray diffraction (XRD), transmission electron microscopy (TEM), dynamic light scattering (DLS) measurements, Fourier transform infrared spectroscopy (FTIR), thermogravimetric analysis (TGA) and vibrating sample magnetometer (VSM). The as-synthesized SPIONs showed very good water solubility and high magnetization value (Ms = 55-73 emu/g). Furthermore, the as-synthesized ATA-coated SPIONs are conjugated with a fluorophore (Alexa Fluor 488) to demonstrate their ability for further chemical/biological conjugation without any additional surface modifications. Moreover, above 90% cell viability in MCF-7 cancer cells has been observed, thus confirming good cytocompatibility of the SPIONs. Therefore, these hydrophilic and carboxyl-amine functionalized SPIONs are very promising candidates to be used for biomedical applications.

Keywords: **Superparamagnetic Iron Oxide Nanoparticles (SPIONs), Water based Ferrofluid, Functionalized Magnetic Nanoparticles, Chemical Synthesis, Benzene-Carboxylic Acids, and *In vitro* Cytotoxicity**

View Article Online
DOI: 10.1039/C6RA18567C

1. Introduction

Superparamagnetic iron oxide nanoparticles (SPIONs - Fe_3O_4/Fe_2O_3) have garnered a great deal of attention in the biomedical field such as magnetic targeting, magnetofection, cancer hyperthermia therapy, and magnetic resonance imaging (MRI) [1–6]. This is due to their unique physicochemical characteristics, for instance (i) higher chemical stability as compared to the ferromagnetic (Fe, Co, and Ni) nanoparticles (ii) size/shape dependent magnetic properties such as superparamagnetism (under 20 nm) at room temperature, and (iii) biocompatibility, i.e., less cytotoxicity and ability to mix as normal iron ions in blood [7–10].

Among the various synthesis routes, the following two methods are predominantly utilized to prepare the SPIONs: (i) chemical co-precipitation which is a simple, high yield and low cost method; (ii) thermal decomposition/thermolysis which is a high temperature method for producing well-crystalline and highly monodispersed SPIONs [11–15]. It is very important to cover the surface of the SPIONs with a suitable coating molecule mainly to disperse them in an appropriate solvent by preventing their agglomeration, and also to provide the surface functional groups for their further conjugation with other imaging/targeting/therapeutic agents [16–18]. Various hydrophilic surface coating molecules have been extensively used for synthesizing water-soluble SPIONs through the single-step co-precipitation/thermolysis route [19–26]. However, there are many drawbacks for the water-soluble SPIONs such as (i) the long-chained surface coatings form a thick dead magnetic/anti-ferromagnetic layer on the surface of the SPIONs, which has detrimental effects on their magnetic properties [27–29]; (ii) the risk of dissociation of the coating layers and thus chance of reducing the water solubility of the SPIONs; (iii) the toxicity of the surface coating molecules reduces the biocompatibility of the SPIONs; and (iv) most importantly the lack of effective surface functional groups, which demands to perform the tedious and time consuming surface modifications (via ligand exchange/bilayer surfactant stabilization) for further chemical and/or biological conjugation of the SPIONs [30–32]. Therefore, there are still challenges to select the effective surface coating molecules for synthesizing highly water-soluble and surface functionalized SPIONs by one-pot chemical synthesis route without compromising their magnetic properties and biocompatibility.

We have identified benzene carboxylic acid molecules such as terephthalic acid (TA), 2-aminoterephthalic acid (ATA), trimesic acid (TMA) and pyromelltic acid (PMA) (see scheme 1) as the novel and effective surface coatings for synthesizing the SPIONs through the co-

View Article Online
DOI: 10.1039/C6RA18567C

precipitation/thermolysis route due to their following advantages: (i) shorter chain length (approx. 0.8 – 1 nm) which could improve the magnetic properties of the SPIONs; (ii) hydrophilic in nature to provide them better water dispersibility; (iii) less toxic in nature for good cytocompatibility of the SPIONs; (iv) presence of adequate carboxylic (-COOH) and/or amine (-NH_2) groups which could help for in-situ surface functionalization of the SPIONs.

Recently, our group have reported facile synthesis of the water-soluble SPIONs based on the chemical co-precipitation using the TA/ATA surface coating molecules [33]. The TA/ATA coated SPIONs exhibited higher magnetization values (74.3/73.6 emu/g) and MRI relaxivity values (735.3/450.8 mM^{-1} s^{-1}) as compared to the SPIONs reported in the literature [34–39]. In this paper, we have reported the synthesis of the TA, ATA, TMA and PMA coated SPIONs through the thermolysis and/or co-precipitation route using the single or combination of the TA/ATA/TMA/PMA surface coating molecules. The as-synthesized SPIONs have been characterized by X-ray diffraction (XRD), transmission electron microscopy (TEM), dynamic light scattering (DLS) measurements, Fourier transform infrared spectroscopy (FTIR), thermogravimetric analysis (TGA) and vibrating sample magnetometer (VSM) to evaluate their structure, morphology, size distribution, water solubility and magnetic properties. Furthermore, we have conjugated a fluorophore (Alexa Fluor® 488) with the ATA-SPIONs to investigate their potentiality for the chemical/biological conjugation without any additional surface modifications. Finally, the *in vitro* cytotoxicity study for the as-synthesized SPIONs has been performed using trypan blue assay in MCF-7 cancer cells to evaluate their biocompatibility for using them in the biomedical applications.

2. Experimental details

2.1 Materials

Iron (II) chloride tetrahydrate ($FeCl_2.4H_2O$), TA ($C_6H_4(CO_2H)_2$), and 2-ATA (H2NC6H3-1,4-(CO2H)2) are purchased from Sigma Aldrich. Iron (III) acetylacetonate (Fe (acac)3) and Iron(III) chloride hexahydrate ($FeCl_3.6H_2O$) are obtained from Spectrochem and Loba chemicals respectively. TMA ($C_6H_4(CO_2H)3$) and PMA ($C_6H_4(CO_2H)4$) are purchased from Alfa Aesar. Ammonium hydroxide (NH4OH - 25 % in H2O), Triethylene glycol (C6H14O4), Alexa Fluor® 488 carboxylic acid–succinimidyl ester and Nitric acid are obtained

View Article Online
DOI: 10.1039/C6RA18567C

from Thermo Fisher Scientific. All the purchased chemicals are analytical grade and used as received.

2.2 Synthesis routes

2.2.1 Chemical co-precipitation

Initially, SPIONs are synthesized by chemical co-precipitation as reported elsewhere [33]. For TMA-coated water-dispersible SPIONs, 1.17 g of $FeCl_3.6H_2O$, 0.43 g of $FeCl_2.4H_2O$ and 0.945 g of TMA are added to a 100 ml round bottom flask containing 22.5 ml of distilled water. The reaction mixture is heated to 80 ºC for 60 minutes under nitrogen gas flow and magnetic stirring (400 rpm). Then 2.5 ml of NH_4OH is rapidly added to the reaction mixture, which is then vigorously stirred (1000 rpm) for next 60 minutes at 80 ºC and then cooled down to room temperature. The resultant black SPIONs are magnetically separated and washed with ethanol/distilled water. Finally, one half of the washed particles is re-dispersed in distilled water to get ferrofluid samples and the other half is dried overnight in a hot air oven at 40 °C to obtain dry sample of the TMA-coated SPIONs (hereafter marked as S1) for further characterizations. Similar procedure is followed to prepare the PMA-coated SPIONs (S2). However, 4.5 ml of NH_4OH (25 % in H_2O) is used to maintain pH at 10-11 necessary to initiate the nucleation of the SPIONs. In similar fashion, ATA is combined with TA, TMA and PMA at equal ratios for synthesizing the ATA-TA, ATA-TMA and ATA-PMA coated SPIONs (S3, S4 and S5) respectively. All the prepared samples are enlisted in Table 1.

2.2.2 Thermal decomposition

Hydrophilic SPIONs are synthesized separately using the surfactants such as TA, ATA, TMA and PMA through the thermal decomposition method also. Typically 2 mmol of $Fe(acac)_3$ is dissolved in 20 ml of TEG along with 6 mmol of the corresponding surfactant in a 150 ml round bottom flask. The flask is dehydrated at 120 °C for 60 minutes in the presence of nitrogen. Then, the flask is quickly heated and maintained at a refluxing temperature of 280 °C (for TA, ATA and TMA) and 250 °C (for PMA) for another 60 minutes to prepare SPIONs. It has been noted that there is no formation of SPIONs in case of the synthesis using PMA, which could be due to the increased acidic environment. Thus, only the TA-, ATA- and TMA-coated SPIONs (S6, S7 and S8 respectively) are obtained.

View Article Online
DOI: 10.1039/C6RA18567C

Next, similar to co-precipitation method, ATA is used in equal ratio (1:1) with TA and TMA to yield ATA-TA and ATA-TMA coated SPIONs (S9 and S10 respectively) via the same method. However, SPIONs have not formed while using ATA-PMA, which is similar to the case of PMA-based synthesis. All the SPIONs (S6-S10) are magnetically separated and washed with ethanol/water. The prepared samples are enlisted in Table 1.

2.3 Characterization

SPIONs are characterized for morphology (size/shape) by using transmission electron microscope (TEM, Technai G2 20 S-TWIN) and for phase purity/crystallite size by using X-ray diffraction (XRD, Bruker D8 Advance – CuKα (λ = 1.54 nm)). The hydrodynamic size and zeta potentials are measured using dynamic light scattering (DLS, Horiba nanoPartica SZ-100-Z). The organic surface coatings adsorbed to the surface of SPIONs are investigated via Fourier transform infrared spectrometer (FTIR, ThermoFisher Scientific Nicolet™ iS™ 5), and thermogravimetric analysis (TGA, SII 6300 EXSTAR). The magnetic properties of the SPIONs are studied using vibrating sample magnetometer (VSM, PAR 155) at room temperature.

Moreover, the final iron concentrations of the as-synthesized SPIONs are measured using atomic absorption spectrometer (AAS) [40]. Herein, a known amount of the SPIONs is mixed with 2 ml of conc. nitric acid and heated to 110 °C for 45 mins. Then the final samples are diluted with sufficient DW and analyzed using AAS (Avanta M). The samples are investigated in comparison with the iron AAS standard (Fisher Scientific).

2.4 Conjugation

The attachment of Alexa Fluor® 488 carboxylic acid–succinimidyl ester (an amine reactive fluorophore) with ATA-coated SPIONs (S7 – synthesized via thermolysis process) is performed based on a modified conjugation method [41]. Briefly, 100 µl of magnetically separated SPIONs is thoroughly mixed with an equal amount of freshly prepared 0.1 M sodium bicarbonate buffer. Then, 1 µl of known concentration of fluorophore is added to the above mixture, vortexed and incubated in ice for 3 h. Later, the mixture is centrifuged, washed thrice with buffer and separated magnetically to remove excess fluorophore. Then, the final mixture is resuspended in buffer and stored at -20 °C for further characterization with the Flourimeter (Horiba Fluorolog®-3)) to confirm the conjugation of the fluorophore with the

View Article Online
DOI: 10.1039/C6RA18567C

functional groups of the ATA coated SPIONs. Similar procedure is followed except the addition of the fluorophore for the unconjugated ATA-SPIONs.

2.5 In vitro cell viability

The cell viability of the as-synthesized SPIONs in the MCF-7 breast cancer cells is analyzed by trypan blue assay (HiMedia), since it is considered to be one of the gold-standard methods to determine the viability of magnetic nanoparticles [22,42,43]. The MCF-7 cancer cells (originally obtained from the American Type Culture Collection (ATCC, Catalog number HTB-22^{TM}) are authenticated and generously provided to us by Dr. Soumya Sinha Roy, Institute of Genomics and Integrative Biology (CSIR-IGIB), India). Samples are incubated with MCF-7 cancer cells (35,000 cells per well) at concentrations ranging from 2.5 - 25 μg_{Fe}/well for 24 h at 37 °C under 5% CO_2. After the incubation period, cells are washed with phosphate buffer saline (PBS - HiMedia) for 3 times, trypsinized and resuspended in media (Gibco, Invitrogen). Then, small aliquots of MCF-7 cell suspensions are added to an equal volume of 0.5% trypan blue and gently mixed. Finally, the number of live to dead cells is counted under a microscope (Leica MC120) by using a hemocytometer (Marienfeld, Germany) [44,45]. The viability is determined in triplicates using the following formula.

Cell Viability (in %) = 100* ((No. of Unstained cells) / (No. of Unstained and Stained cells))

3. Results and discussions

3.1 Crystal structure

Fig. 1 depicts the XRD pattern of the as-synthesized SPIONs (S6 sample). The positions of the diffraction peaks (220), (311), (400), (422), (511), (440) and (533) are in good agreement with those of the standard XRD patterns for magnetite (Fe_3O_4) phase (JCPDS File no.19-0629), and also confirming the spinel structure of SPIONs [33]. Similar XRD patterns are observed for the other samples (data not shown). Moreover, the average crystallite sizes for all the samples (S1-S10) are calculated from the obtained XRD patterns using Scherrer equation (which is $D = K\lambda/(\beta\cos\theta)$, where K is constant, λ is X-ray wavelength, and β is the peak width of half-maximum) by considering diffraction peaks corresponding to the (311) plane [46,47]. The calculated crystallite sizes of the respective SPIONs are listed in Table 1 for comparison.

View Article Online
DOI: 10.1039/C6RA18567C

3.2 Size and morphology

Fig. 2A and 2B show the TEM images of the respective samples of SPIONs. The average particle sizes (by considering at least 50 particles in each case) of the SPIONs are determined using Image J software [48]. The average particle sizes and shapes of the respective SPIONs are listed in Table 1. The TEM sizes are in the range of 7-9 nm and 5-11 nm for the SPIONs synthesized via chemical co-precipitation and thermal decomposition methods respectively, which indicate that the nanoparticles are in the superparamagnetic regime [12]. Moreover, the TEM sizes of the SPIONs are very close to their crystallite size (as calculated from XRD pattern), which indicate the nearly single crystalline nature of the nanoparticles [49].

Furthermore, it can be noted that the particle sizes of the thermolysis based SPIONs (S6-S10 samples) vary with respect to different surface coatings, as compared to the SPIONs (S1-S5 samples) synthesized via co-precipitation process (refer Table 1). This could be due to the influence of high reaction temperature that led to the increased surface reactivity of the SPIONs and the corresponding attachment of the organic molecules to their surface.

It can also be seen that the SPIONs are mostly spherical in shape (S2, S3, S5, S6, S7 and S9). However, spheroidal (in S1, S4, and S10 sample) and mixed (in S8 sample) shapes can also be observed for the respective SPIONs, which could be attributed to the influence of the chemical structure of TMA molecules.

Furthermore, the selected area electron diffraction (SAED) patterns for S4 and S9 samples (refer A1 and A2 from Fig. 2A and 2B respectively) clearly showing that the diffraction rings are due to (220), (311), (400), (511) and (440) lattice planes (which are similar to the XRD patterns of sample S6) [50]. Similar SAED patterns are manifested by the other samples (not shown here). Thus, it has been affirmed again that the as-prepared SPIONs possess the magnetite (Fe_3O_4) phase.

3.3 DLS measurements

Fig. 3, A & C depict DLS size distribution plots of the SPIONs (S1 and S6 samples respectively) in aqueous suspensions, which indicate the narrow size distribution for both the samples. The obtained average hydrodynamic sizes are 10.4 nm and 11.5 nm respectively, which are slightly larger than the average TEM particle sizes (7 and 11 nm respectively), that could be due to the coordination of the organic surface coatings that increases the particle sizes [46].

View Article Online
DOI: 10.1039/C6RA18567C

Moreover, Fig.3, B & D show the zeta potential distribution plots of the SPIONs (for S1 and S6 respectively) in the aqueous suspension. The maxima of the plots are observed at -41.1 and -41.0 mV for the S1 and S6 samples respectively, which reveals that the surfaces of the SPIONs are negatively charged. Usually the nanoparticles with zeta potentials above ±30 mV are noted to be stable, since the high surface electric charge can reduce the aggregation of nanoparticles due to strong repulsive forces [23,51]. Thus, the observed results show that the negatively charges of the as-synthesized SPIONs are adequate to retain them from interacting with each other.

Therefore, a stable particle size and very good colloidal stability/water dispersibility are ascertained for the as-synthesized SPIONs. Similar hydrodynamic sizes and zeta potential values can be obtained for the other samples.

3.4 Surface coatings

3.4.1 FTIR

Fig. S1 (i-v) (refer supplementary information) displays the FTIR spectra of bare SPIONs, ATA, TA, TMA and PMA molecules respectively. Moreover, Fig. 4A (a-e) and Fig. 4B (f-j) show the FTIR spectra of the S1-S5 and S6-S10 samples respectively. In Fig. S1 (i), 4A (a-e) and 4B (f-j), the absorption peaks in the range of 565-588 cm^{-1} belong to the Fe-O stretching vibrations of iron oxide cores, whereas the peaks above 600 cm^{-1} are attributed to the vibrations of the chemically adsorbed surfactants of SPIONs [52–54]. Moreover, in Fig. S1 (ii-v), the absorption peaks at 1493 assigned to N-H bending vibration of ATA, 1673 and 1396 assigned to C=O stretching and O-H bending vibrations of TA, 1605, 1397 and 745 assigned to C=C stretching, O-H bending and C-H bending vibrations of TMA and 1697, 1405 and 862 assigned to C=O stretching, O-H bending and C-H bending vibrations of PMA molecules.

In Fig. 4A (a & d), the absorption peaks at about 1605/1609, 1397, and 756/755 cm^{-1} are due to C=C stretching, O-H bending and C-H bending vibrations of corresponding TMA coatings in S1/S4 respectively. Whereas, the peaks at 1698, 1401 and 858/857 cm^{-1} are associated with C=O stretching, O-H bending and C-H bending vibrations of PMA coatings of S2/S5 correspondingly (refer Fig. 4A (b & e)). The peaks at 1703 and 1398 cm^{-1} are attributed to C=O stretching, and O-H bending vibrations of TA molecules in S3 (refer Fig. 4A (c)). Moreover, the peaks at 1494, 1489, and 1483 cm^{-1} are attributed to N-H bending vibration in the

View Article Online
DOI: 10.1039/C6RA18567C

amino group of ATA molecules, thereby confirming its attachment towards the surface of the respective samples of the SPIONs (i.e., S3, S4 and S5) [55]. Thus, the adsorption of the TMA/PMA/TA/ATA molecules on the surface of respective samples of the SPIONs (prepared by co-precipitation method) is affirmed.

In Fig. 4B (f-h), the absorption peaks at 1716, 1714 and 1709 cm^{-1} are assigned for the C=O stretching vibrations of the carboxylic acid groups corresponding to the TA, ATA, and TMA molecules, respectively. Moreover, the peaks at 753 and 751 cm^{-1} are attributed to the C-H bending vibrations of the TMA coatings of the SPIONs in S8/S10 samples (refer Fig. 4B (h & j)), respectively. Furthermore, the absorption peaks appeared in the region 1400–1600 cm^{-1} are corresponding to the symmetric and asymmetric vibrations of the amino groups of ATA molecules in S7/S9/S10 samples (refer Fig. 4B (h-j)) [33]. Thus, the presence of TA/ATA/TMA coatings on the surface of the respective SPIONs (synthesized by thermolysis method) is confirmed.

3.4.2 TGA

The amounts of the surface coatings for all the SPIONs (prepared using co-precipitation and thermolysis method) are estimated by TGA measurements, as shown in Fig. 5 (A and B respectively). The TGA curves show two weight-losses when the samples are heated from room temperature to 700°C in the nitrogen atmosphere at the rate of 10 °C/min. The primary weight loss in the temperature range of 25-200°C is due to the evaporation of water, whereas the secondary weight loss (in the temperature range of 200-700 °C) is due to the decomposition of the respective organic surface coatings (TMA, PMA, TA and ATA) of the SPIONs [16]. The amount of the secondary weight losses for all the samples is listed in Table 1. It can be noted that the amount of surface coating is higher for the SPIONs prepared by the thermolysis method as compared to those prepared by the co-precipitation method, which could be due to the higher reaction temperature (for thermolysis) that enforces more surface adsorption of the coating molecules to the SPIONs.

Therefore, the FTIR spectra and TGA curves confirm that the surfaces of the SPIONs are attached with corresponding surface coating molecules (TMA/PMA/TA/ATA).

View Article Online
DOI: 10.1039/C6RA18567C

3.5 Magnetic properties

In Fig. 6, A and B show the magnetization (M–H) curves of samples of the SPIONs (synthesized via co-precipitation and thermolysis methods) from S1-S5 and S6-S10 respectively at room temperature. The zero/negligible coercivity and residual magnetization of all the M-H curves confirm that all the SPIONs samples are superparamagnetic in nature at the room temperature. The saturation magnetization (M_s) values of all the SPIONs are listed in Table 1. The M_s values are found to be in the range of 58.29 - 66.30 emu/g and 11.74 - 73.09 emu/g (refer Table 1) for the SPIONs prepared by the co-precipitation and thermolysis route respectively.

Moreover, it can be observed that the M_s values of the SPIONs (e.g. 73.60, 58.29, 66.30, and 61.83 emu/g for S0*, S1, S3 and S4 samples respectively) synthesized via the co-precipitation method are higher than that of those prepared by the thermolysis (e.g. 55.9, 11.74, 64.70 and 34.64 emu/g for S7, S8, S9 and S10 samples respectively). As compared to the co-precipitation method, the SPIONs formed by thermolysis method showed reduction in Ms values, which could be mainly due to the following reasons: (i) reduced sizes (i.e., 7±4, 5±2, 8±4 and 6±3 nm for S7, S8, S9 and S10 samples respectively) and (ii) higher adsorption of organic surface coatings as confirmed by the TGA data in Table 1 (i.e., 14, 52.1, 10 and 43.5 wt % for ATA, TMA, ATA-TA and ATA-TMA coated SPIONs respectively). It is in good agreement with the previous reports that the M_s value decreases with (i) decrease in the particle size of the SPIONs and (ii) increase in the amount of non-magnetic surface coatings [23,56].

However, S6 sample (prepared from thermolysis method) possesses the highest M_s value (73.09 emu/g) regardless of the large amount of organic molecules (27 wt %) on its surface, which could be due to the increase in their size (11±2 nm) as compared to the other samples of SPIONs.

In addition, it can also be seen that the magnetization values of the dual-surfactants coated SPIONs (i.e., 61.83, 63.2, 64.70 and 34.64 emu/g for S4, S5, S9 and S10 samples respectively) are comparatively higher than that the single-surfactant coated nanoparticles (i.e., 58.29, 62.26, 55.90 and 11.74 emu/g for S1, S2 S7 and S8 respectively), which could be attributed to the enhanced crystallinity with respect to the compact arrangement of ATA along with the respective surfactants on the surface of SPIONs [57]. Thus, it can be concluded that the preparation methods and/or surfactants (individually and/or combination) can influence the

View Article Online
DOI: 10.1039/C6RA18567C

magnetic properties (especially on M_s values) of the SPIONs with respect to their morphology and the amount of surface coatings.

However, the Ms values (11.74 - 73.9 emu/g) of all the samples are lower than the theoretical value (92 emu/g) of bulk magnetite, which can be either due to (i) the differences in order–disorder characteristics based on nanoparticle formation mechanisms and/or (ii) the presence of non-collinear spins on the surface of SPIONs due to surfactants [58,59]. Nevertheless, the Ms values of the as-prepared SPIONs are similar/higher than many recently reported SPIONs samples, which have already been tested for their efficacy in biomedical applications [35,60–70].

3.6 Photoluminescence of fluorophore conjugated nanoparticles

Fig 7 (i) shows the possible mechanism for conjugation of the Alexa Fluor® 488 carboxylic acid–succinimidyl ester with the ATA-SPIONs (S7), where the amide bond is formed between the fluorophore and amine groups located on ortho position of the ATA molecules (whose carboxylate group is attached to the surface of the SPIONs). Fig. 7 (ii), (a), (b) and (c) show the photoluminescence (PL) spectra of the Alexa Fluor® 488 fluorophore-conjugated SPIONs, unconjugated SPIONs and the buffer respectively (under the excitation at 488 nm). It can be noted that there is a significant increase in the intensity of the fluorophore-conjugated SPIONs (Fig. 7 (ii) - a) as compared to the unconjugated ATA-SPIONs (Fig. 7 (ii) - b) and only buffer (Fig. 7 (ii) - c). Thus, the PL spectrum confirms the fluorophore conjugation with the ATA-SPIONs using the $-NH_2$ functional groups.

3.7 In vitro cytotoxicity

The *in vitro* cytotoxicity of the selected SPIONs samples (i.e., S1-S7 and S9 having M_s value above 55 emu/g) is analyzed on the MCF-7 breast cancer cell lines via trypan blue assay at different concentrations (2.5 - 25 μg_{Fe}/well). The cytotoxicity results of the SPIONs are plotted against the control cells (untreated with SPIONs), where the cell viability is considered as 100% (see Fig. 8A and Fig. 8B). It can be observed that all the SPIONs (S1-S7 and S9 samples) exhibit excellent cell viability of above 90 % in the concentration range of 2.5 - 25 μg_{Fe}/well. Therefore, the selected water-soluble SPIONs are highly biocompatible in MCF-7 cancer cells. Moreover, the morphological changes in the MCF-7 cells after 24 h treatment with the samples of SPIONs (from S1-S7 and S9) are also investigated after washing them 3 times with PBS [71]. Negative or

View Article Online
DOI: 10.1039/C6RA18567C

very trivial alterations in the morphology of treated MCF-7 cells are noticed as compared to the untreated control cells as per the microscopic images (refer Fig. 9). Moreover, it can be noted that the accumulation of the nanoparticles inside the cancer cells (as confirmed by Prussian blue staining method - data not shown) is increased with the concentrations of the SPIONs (from 2.5 - 25 μg_{Fe}/well) that could be promising for cancer hyperthermia applications.

4. Conclusion

To summarize, we have successfully synthesized the hydrophilic and carboxyl-amine functionalized SPIONs using the novel surfactant molecules such as TA/ATA/TMA/PMA (single surfactant) and their combination (dual surfactant) by one-step facile chemical co-precipitation/thermolysis route. The as-synthesized SPIONs showed very good water solubility and high magnetization value (Ms = 55-73 emu/g for S1-S7 and S9 samples). The highest Ms value is obtained for the TA-SPIONs (73.09 emu/g for S6 sample), synthesized using the thermal decomposition method. Moreover, the facile conjugation of the fluorophore (Alexa Fluor 488) is demonstrated without any additional surface modifications for the as-synthesized ATA-SPIONs. Furthermore, the SPIONs (S1-S7 and S9 with high M_s values) showed very good cytocompatibility (above 90%) to the MCF-7 breast cancer cells. Thus, these novel hydrophilic and carboxyl-amine functionalized SPIONs are very promising candidates to be used for the biomedical applications. Our future studies are aimed to investigate the efficacy of these SPIONs (with/without chemical/biological conjugation) in *in vitro/in vivo* MR imaging and magnetic hyperthermia therapy for the cancer treatments.

ACKNOWLEDGEMENTS

The financial support from the Department of Science and Technology (DST) under Nanomission, New Delhi, India (Grant No: SR/NM/NS-1141/2015 (G)) is gratefully acknowledged. Fruitful discussions with Dr. Goutam Chowdhury and Dr. Koyeli Mapa are acknowledged. We also thank IIT Roorkee and IIT Mandi for providing instrumental facilities.

View Article Online
DOI: 10.1039/C6RA18567C

REFERENCES

1 A. Saraswathy, S. S. Nazeer, M. Jeevan, N. Nimi, S. Arumugam, V. S. Harikrishnan, P. R. H. Varma and R. S. Jayasree, *Colloids Surfaces B Biointerfaces*, 2014, **117**, 216–224.

2 A. K. Swain, L. Pradhan and D. Bahadur, *ACS Appl. Mater. Interfaces*, 2015, **7**, 8013–8022.

3 M. Takafuji, K. Kitaura, T. Nishiyama, S. Govindarajan, V. Gopal, T. Imamura and H. Ihara, *J. Mater. Chem. B*, 2014, **2**, 644.

4 M. L. Mojica Pisciotti, E. Lima, M. Vasquez Mansilla, V. E. Tognoli, H. E. Troiani, a. a. Pasa, T. B. Creczynski-Pasa, a. H. Silva, P. Gurman, L. Colombo, G. F. Goya, A. Lamagna and R. D. Zysler, *J. Biomed. Mater. Res. - Part B Appl. Biomater.*, 2014, **102**, 860–868.

5 S. Prijic, L. Prosen, M. Cemazar, J. Scancar, R. Romih, J. Lavrencak, V. B. Bregar, A. Coer, M. Krzan, A. Znidarsic and G. Sersa, *Biomaterials*, 2012, **33**, 4379–4391.

6 S. Sharifi, H. Seyednejad, S. Laurent, F. Atyabi, A. A. Saei and M. Mahmoudi, *Contrast Media Mol. Imaging*, 2015, n/a-n/a.

7 R. Weissleder, D. D. Stark, B. L. Engelstad, B. R. Bacon, D. L. White, P. Jacobs and J. Lewis, *Am. J. Roentgenol.*, 1989, **152**, 167–173.

8 P. Guardia, A. Labarta and X. Batlle, *J. Phys. Chem. C*, 2011, **115**, 390–396.

9 S. Laurent, D. Forge, M. Port, A. Roch, C. Robic, L. Vander Elst and R. N. Muller, *Chem. Rev.*, 2008, **108**, 2064–2110.

10 D. Wang, Q. Ma and P. Yang, *J. Nanosci. Nanotechnol.*, 2012, **12**, 6432–6438.

11 D. Maity and J. Ding, *Int. J. Nanosci.*, 2011, **10**, 943–947.

12 R. Hachani, M. Lowdell, M. Birchall, A. Hervault, D. Mertz, S. Begin-Colin and N. T. K. Thanh, *Nanoscale*, 2016, **8**, 3278–3287.

13 W. Wu, Z. Wu, T. Yu, C. Jiang and W.-S. Kim, *Sci. Technol. Adv. Mater.*, 2015, **16**, 23501.

14 M. Faraji, Y. Yamini and M. Rezaee, *J. Iran. Chem. Soc.*, 2010, **7**, 1–37.

15 S. F. Hasany, I. Ahmed, R. J and a. Rehman, *Nanosci. Nanotechnol.*, 2013, **2**, 148–158.

16 D. Maity, S. G. Choo, J. Yi, J. Ding and J. M. Xue, *J. Magn. Magn. Mater.*, 2009, **321**, 1256–1259.

17 W. Wu, Q. He and C. Jiang, *Nanoscale Res. Lett.*, 2008, **3**, 397–415.

18 M. Mahmoudi, S. Sant, B. Wang, S. Laurent and T. Sen, *Adv. Drug Deliv. Rev.*, 2011, **63**, 24–46.

19 A. K. L. Yuen, G. A. Hutton, A. F. Masters and T. Maschmeyer, *Dalt. Trans.*, 2012, 41, 2545.

View Article Online
DOI: 10.1039/C6RA18567C

20 K. Turcheniuk, A. V Tarasevych, V. P. Kukhar, R. Boukherroub and S. Szunerits, *Nanoscale*, 2013, **5**, 10729.

21 E. Amstad, T. Gillich, I. Bilecka, M. Textor and E. Reimhult, *Nano Lett.*, 2009, **41**, 4042–4048.

22 D. Maity, P. Chandrasekharan, P. Pradhan, K.-H. Chuang, J.-M. Xue, S.-S. Feng and J. Ding, *J. Mater. Chem.*, 2011, **21**, 14717.

23 D. Maity, P. Chandrasekharan, C.-T. Yang, K.-H. Chuang, B. Shuter, J.-M. Xue, J. Ding and S.-S. Feng, *Nanomedicine*, 2010, **5**, 1571–1584.

24 A. Szpak, S. Fiejdasz, W. Prendota, T. Strączek, C. Kapusta, J. Szmyd, M. Nowakowska and S. Zapotoczny, *J. Nanoparticle Res.*, 2014, **16**, 2678.

25 A. M. Kruse, S. A. Meenach, K. W. Anderson and J. Z. Hilt, *Acta Biomater.*, 2014, **10**, 2622–2629.

26 N. Mir, M. Bahrami, E. Safari and S. M. Hosseinpour-Mashkani, *J. Clust. Sci.*, 2015, **26**, 1103–1113.

27 H. Tumturk, F. Sahin and E. Turan, *Analyst*, 2014, **139**, 1093–100.

28 A. H. Lu, E. L. Salabas and F. Schüth, *Angew. Chemie - Int. Ed.*, 2007, **46**, 1222–1244.

29 T. Lam, P. Pouliot, P. K. Avti, F. Lesage and A. K. Kakkar, *Adv. Colloid Interface Sci.*, 2013, **199–200**, 95–113.

30 W. Wang, X. Ji, H. Bin Na, M. Safi, A. Smith, G. Palui, J. M. Perez and H. Mattoussi, *Langmuir*, 2014, **30**, 6197–6208.

31 J. Fouineau, K. Brymora, L. Ourry, F. Mammeri, N. Yaacoub, F. Calvayrac, S. Ammar-Merah and J. M. Greneche, *J. Phys. Chem. C*, 2013, **117**, 14295–14302.

32 E. D. Smolensky, H. Y. E. Park, T. S. Berquó and V. C. Pierre, *Contrast Media Mol. Imaging*, 2011, **6**, 189–199.

33 D. Maity, G. Zoppellaro, V. Sedenkova, J. Tucek, K. Safarova, K. Polakova, K. Tomankova, C. Diwoky, R. Stollberger, L. Machala and R. Zboril, *Chem. Commun. (Camb).*, 2012, **48**, 11398–400.

34 V. Sreeja, K. N. Jayaprabha and P. A. Joy, *Appl. Nanosci.*, 2015, **5**, 435–441.

35 J. Wang, B. Zhang, L. Wang, M. Wang and F. Gao, *Mater. Sci. Eng. C*, 2015, **48**, 416–423.

36 M. Shen, H. Cai, X. Wang, X. Cao, K. Li, S. H. Wang, R. Guo, L. Zheng, G. Zhang and X. Shi, *Nanotechnology*, 2012, **23**, 105601.

37 C. Corot, P. Robert, J. M. Idée and M. Port, *Adv. Drug Deliv. Rev.*, 2006, **58**, 1471–1504.

38 V. Pourcelle, S. Laurent, A. Welle, N. Vriamont, D. Stanicki, L. Vander Elst, R. N. Muller and J. Marchand-Brynaert, *Bioconjug. Chem.*, 2015, **26**, 822–829.

39 L. Xiao, J. Li, D. F. Brougham, E. K. Fox, N. Feliu, A. Bushmelev, A. Schmidt, N. Mertens, F. Kiessling, M. Valldor, B. Fadeel and S. Mathur, *ACS Nano*, 2011, **5**, 6315–

View Article Online
DOI: 10.1039/C6RA18567C

6324.

40 C. Prashant, M. Dipak, C. T. Yang, K. H. Chuang, D. Jun and S. S. Feng, *Biomaterials*, 2010, **31**, 5588–5597.

41 V. Voliani, S. Luin, F. Ricci and F. Beltram, *Nanoscale*, 2010, **2**, 2783–2789.

42 M. Calero, M. Chiappi, A. Lazaro-Carrillo, M. J. Rodríguez, F. J. Chichón, K. Crosbie-Staunton, A. Prina-Mello, Y. Volkov, A. Villanueva and J. L. Carrascosa, *J. Nanobiotechnology*, 2015, **13**, 16.

43 D. Couto, M. Freitas, V. Vilas-Boas, I. Dias, G. Porto, M. A. Lopez-Quintela, J. Rivas, P. Freitas, F. Carvalho and E. Fernandes, *Toxicol. Lett.*, 2014, **225**, 57–65.

44 P. Bhatnagar, M. Alauddin, J. a Bankson, D. Kirui, P. Seifi, H. Huls, D. a Lee, A. Babakhani, M. Ferrari, K. C. Li and L. J. N. Cooper, *Sci. Rep.*, 2014, **4**, 4502.

45 S. Kanagesan, M. Hashim, S. Tamilselvan, N. B. Alitheen, I. Ismail, A. Hajalilou and K. Ahsanul, *Adv. Mater. Sci. Eng.*, 2013, **2013**, 1–7.

46 D. Maity, S. N. Kale, R. Kaul-Ghanekar, J. M. Xue and J. Ding, *J. Magn. Magn. Mater.*, 2009, **321**, 3093–3098.

47 Y. Liu, Y. Li, X. M. Li and T. He, *Langmuir*, 2013, **29**, 15275–15282.

48 H. Unterweger, R. Tietze, C. Janko, J. Zaloga, S. Lyer, S. Dürr, N. Taccardi, O. M. Goudouri, A. Hoppe, D. Eberbeck, D. W. Schubert, A. R. Boccaccini and C. Alexiou, *Int. J. Nanomedicine*, 2014, **9**, 3659–3676.

49 T. Ozkaya, M. S. Toprak, A. Baykal, H. Kavas, Y. Köseoğlu and B. Aktaş, *J. Alloys Compd.*, 2009, **472**, 18–23.

50 S. Ge, X. Shi, K. Sun, C. Li, J. R. Baker, M. M. Banaszak Holl and B. G. Orr, *J. Phys. Chem. C*, 2009, **113**, 13593–13599.

51 B. Banerji, S. K. Pramanik, S. Mandal, N. C. Maiti and K. Chaudhuri, *RSC Adv.*, 2012, **2**, 2493.

52 N. V. Jadhav, A. I. Prasad, A. Kumar, R. Mishra, S. Dhara, K. R. Babu, C. L. Prajapat, N. L. Misra, R. S. Ningthoujam, B. N. Pandey and R. K. Vatsa, *Colloids Surfaces B Biointerfaces*, 2013, **108**, 158–168.

53 L. Hu, A. Percheron, D. Chaumont and C. H. Brachais, *J. Sol-Gel Sci. Technol.*, 2011, **60**, 198–205.

54 M. Bloemen, W. Brullot, T. T. Luong, N. Geukens, A. Gils and T. Verbiest, *J. Nanoparticle Res.*, 2012, **14**.

55 Z. Chen, Q. Zhang, L. Huang, R. Li, W. Li, G. Xu and H. Cheng, *J. Phys. Chem. C*, 2014, **118**, 21244–21249.

56 H. Li, Z. Lu, G. Cheng, K. Rong, F. Chen and R. Chen, *RSC Adv.*, 2015, **5**, 5059–5067.

57 G. Kandasamy and D. Maity, *Int. J. Pharm.*, 2015, **496**, 191–218.

58 M. Wu, D. Zhang, Y. Zeng, L. Wu, X. Liu and J. Liu, *Nanotechnology*, 2015, **26**, 115102.

View Article Online
DOI: 10.1039/C6RA18567C

59 I. O. Perez De Berti, M. V Cagnoli, G. Pecchi, J. L. Alessandrini, S. J. Stewart, J. F. Bengoa and S. G. Marchetti, *Nanotechnology*, 2013, **24**, 175601.

60 B. H. Kim, N. Lee, H. Kim, K. An, Y. Il Park, Y. Choi, K. Shin, Y. Lee, S. G. Kwon, H. Bin Na, J.-G. Park, T.-Y. Ahn, Y.-W. Kim, W. K. Moon, S. H. Choi and T. Hyeon, *J. Am. Chem. Soc.*, 2011, **133**, 12624–12631.

61 S. R. Kumar, L. Marianna, S. Gianni, a J. Nathanael, S. I. Hong, T. Hwan Oh, D. Mangalaraj, C. Viswanathan and N. Ponpandian, *Mater. Res. Express*, 2014, **1**, 15015.

62 B. Luigjes, S. M. C. Woudenberg, R. De Groot, J. D. Meeldijk, H. M. Torres Galvis, K. P. De Jong, A. P. Philipse and B. H. Erné, *J. Phys. Chem. C*, 2011, **115**, 14598–14605.

63 X.-X. Zhang, H. S. Eden and X. Chen, *J. Control. Release*, 2012, **159**, 2–13.

64 M. Song, Y. Zhang, S. Hu, L. Song, J. Dong, Z. Chen and N. Gu, *Colloids Surfaces A Physicochem. Eng. Asp.*, 2012, **408**, 114–121.

65 P. I P Soares, F. Lochte, C. Echeverria, L. C J Pereira, J. T Coutinho, I. M M Ferreira, C. M M Novo and J. P M R Borges, *Nanotechnology*, 2015, **26**, 425704.

66 S. Sadhasivam, S. Savitha, C.-J. Wu, F.-H. Lin and L. Stobiński, *Int. J. Pharm.*, 2015, **480**, 8–14.

67 J. Varshosaz, H. Sadeghi-Aliabadi, S. Ghasemi and B. Behdadfar, *Biomed Res. Int.*, 2013, **2013**.

68 F. Ye, S. Laurent, A. Fornara, L. Astolfi, J. Qin, A. Roch, A. Martini, M. S. Toprak, R. N. Muller and M. Muhammed, *Contrast Media Mol. Imaging*, 2012, **7**, 460–468.

69 M. Filippousi, M. Angelakeris, M. Katsikini, E. Paloura, I. Efthimiopoulos, Y. Wang, D. Zamboulis and G. Van Tendeloo, *J. Phys. Chem. C*, 2014, **118**, 16209–16217.

70 J. J. Ibarra-Sánchez, R. Fuentes-Ramírez, A. G. Roca, M. del Puerto Morales and L. I. Cabrera-Lara, *Ind. Eng. Chem. Res.*, 2013, **52**, 17841–17847.

71 J. Majeed, L. Pradhan, R. S. Ningthoujam, R. K. Vatsa, D. Bahadur and A. K. Tyagi, *Colloids Surfaces B Biointerfaces*, 2014, **122**, 396–403.

View Article Online
DOI: 10.1039/C6RA18567C

Table 1: Surface coatings, XRD crystallite size, TEM size, shape, saturation magnetization and TGA secondary weight loss of the respective SPIONs synthesized via chemical co-precipitation and thermal decomposition methods. [S0 and S0* are TA and ATA coated SPIONS as reported elsewhere [33]]

Samples of SPIONs	Synthesis Method and Reaction Temperature	Surfactants Used	XRD Size (nm)	TEM Size (nm)	Shape	Ms (emu/g)	TGA – Secondary Weight Loss (approx. in %)	Ref
S0	Chemical Co-precipitation and 80 °C	TA	8.23	10±4	Spherical	74.30	2.5	[33]
S0*		ATA	7.65	10±3	Spherical	73.60	2.5	
S1		TMA	8.86	7±3	Spheroid	58.29	4.5	This Work
S2		PMA	10.2	8±3	Spherical	62.26	3.0	
S3		ATA-TA	9.03	9±3	Spherical	66.30	8.6	
S4		ATA-TMA	9.82	9±2	Spheroid	61.83	5.5	
S5		ATA-PMA	9.15	8±2	Spherical	63.20	2.2	
S6	Thermal decomposition and 280 °C	TA	12.1	11±2	Spherical	73.09	27.5	
S7		ATA	7.95	6±2	Spherical	55.90	14.0	
S8		TMA	6.29	5±2	Mixed	11.74	52.1	
S9		ATA-TA	9.98	8±3	Spherical	64.70	10.0	
S10		ATA-TMA	6.36	7±3	Spheroid	34.64	43.5	

View Article Online
DOI: 10.1039/C6RA18567C

FIGURES & CAPTIONS:

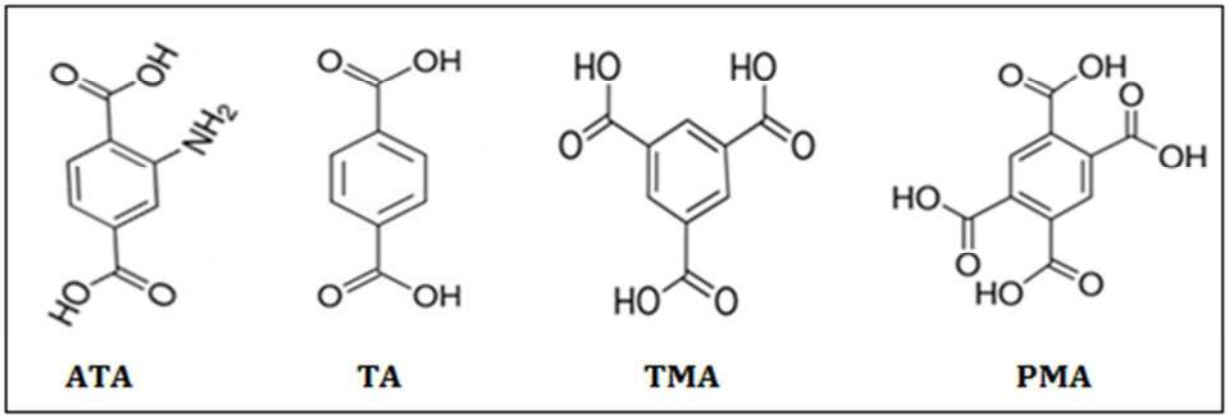

Scheme 1: Molecular structures of terephthalic acid (TA), 2-aminoterephthalic acid (ATA), trimesic acid (TMA) and pyromelltic acid (PMA) molecules.

View Article Online
DOI: 10.1039/C6RA18567C

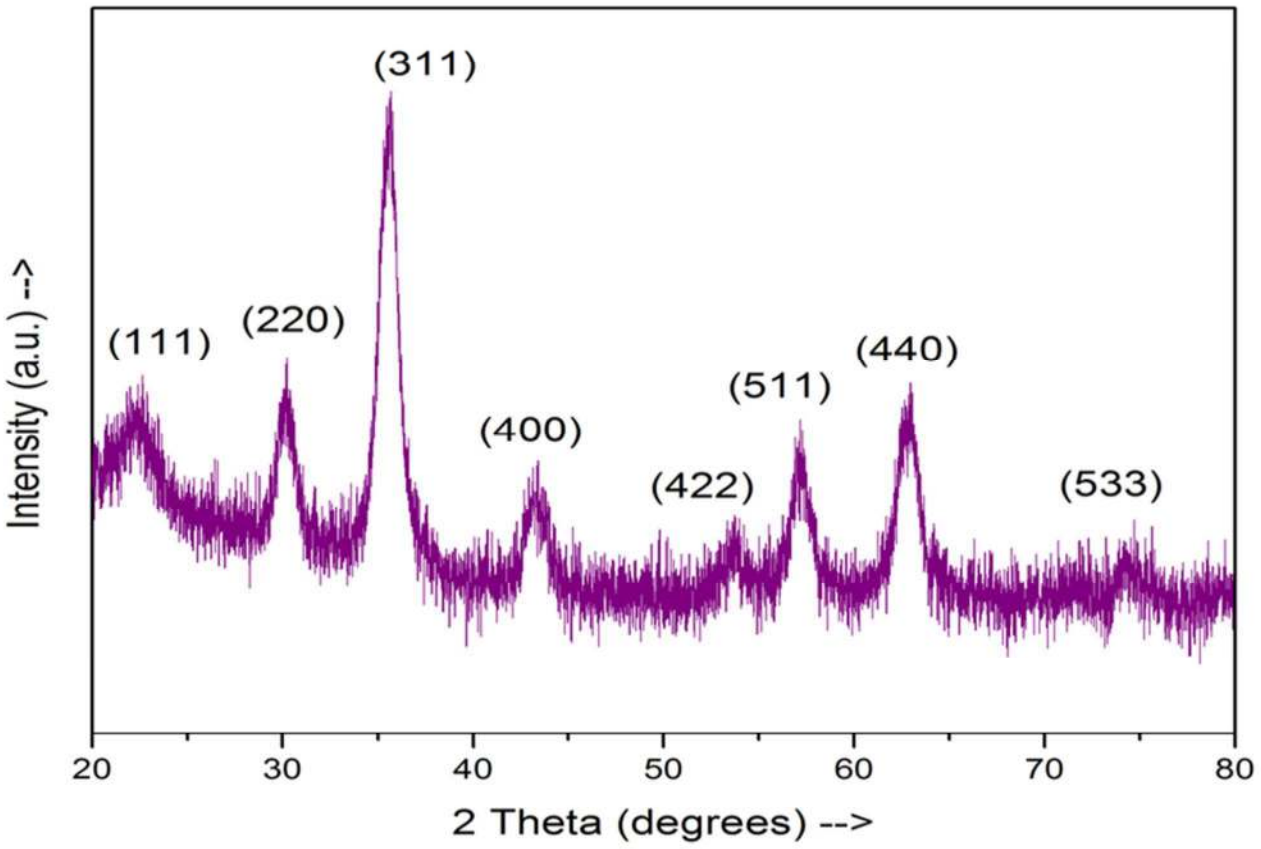

Fig. 1. XRD pattern of the TA-SPIONs (S6).

View Article Online
DOI: 10.1039/C6RA18567C

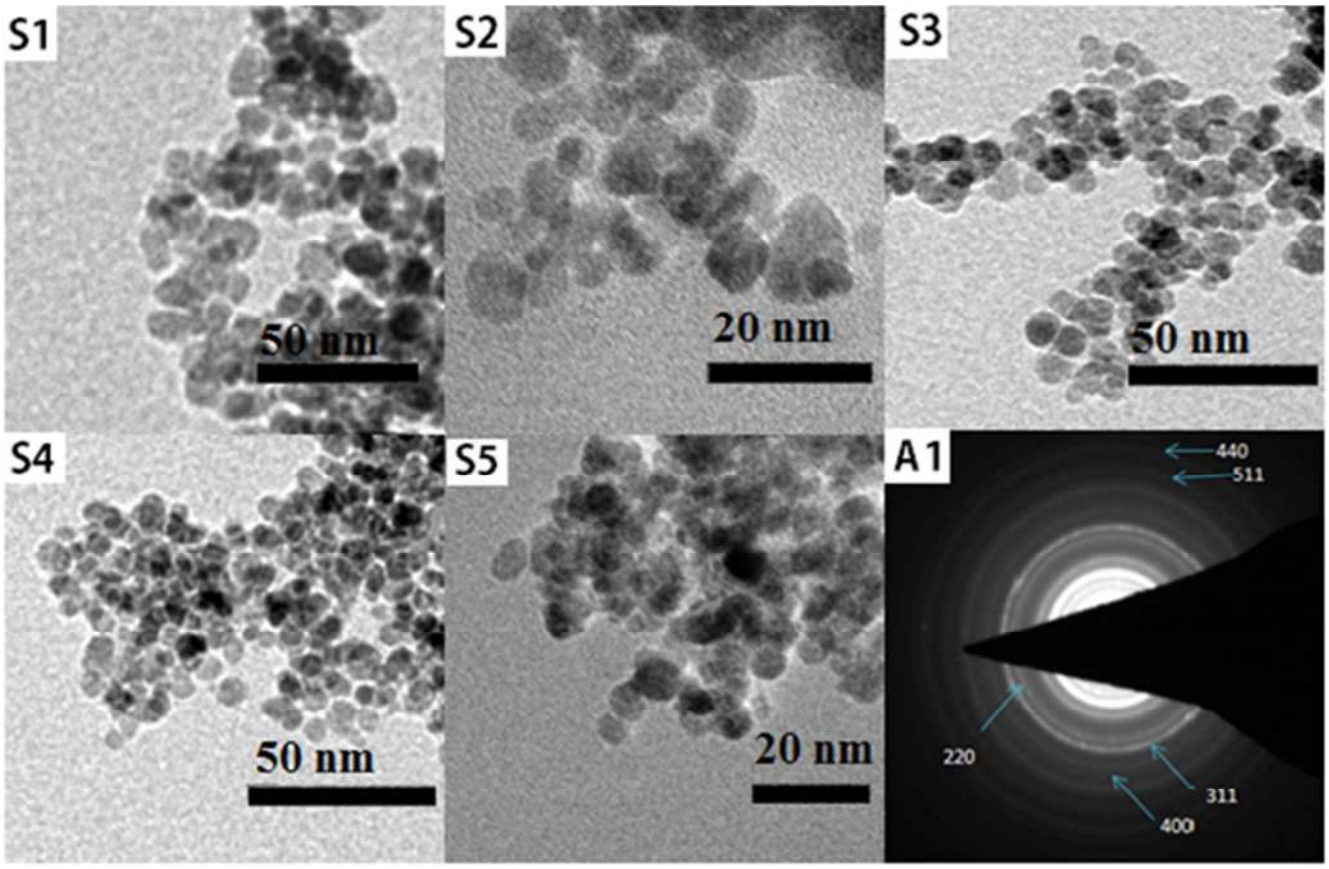

Fig. 2A. TEM images of the TMA-SPIONs (S1), PMA-SPIONs (S2), S3- ATA-TA-SPIONs, ATA-TMA-SPIONs (S4) and ATA-PMA-SPIONs (S5) respectively, synthesized by the chemical co-precipitation method. A1 represents the SAED pattern of the ATA-TMA-SPIONs (S4).

View Article Online
DOI: 10.1039/C6RA18567C

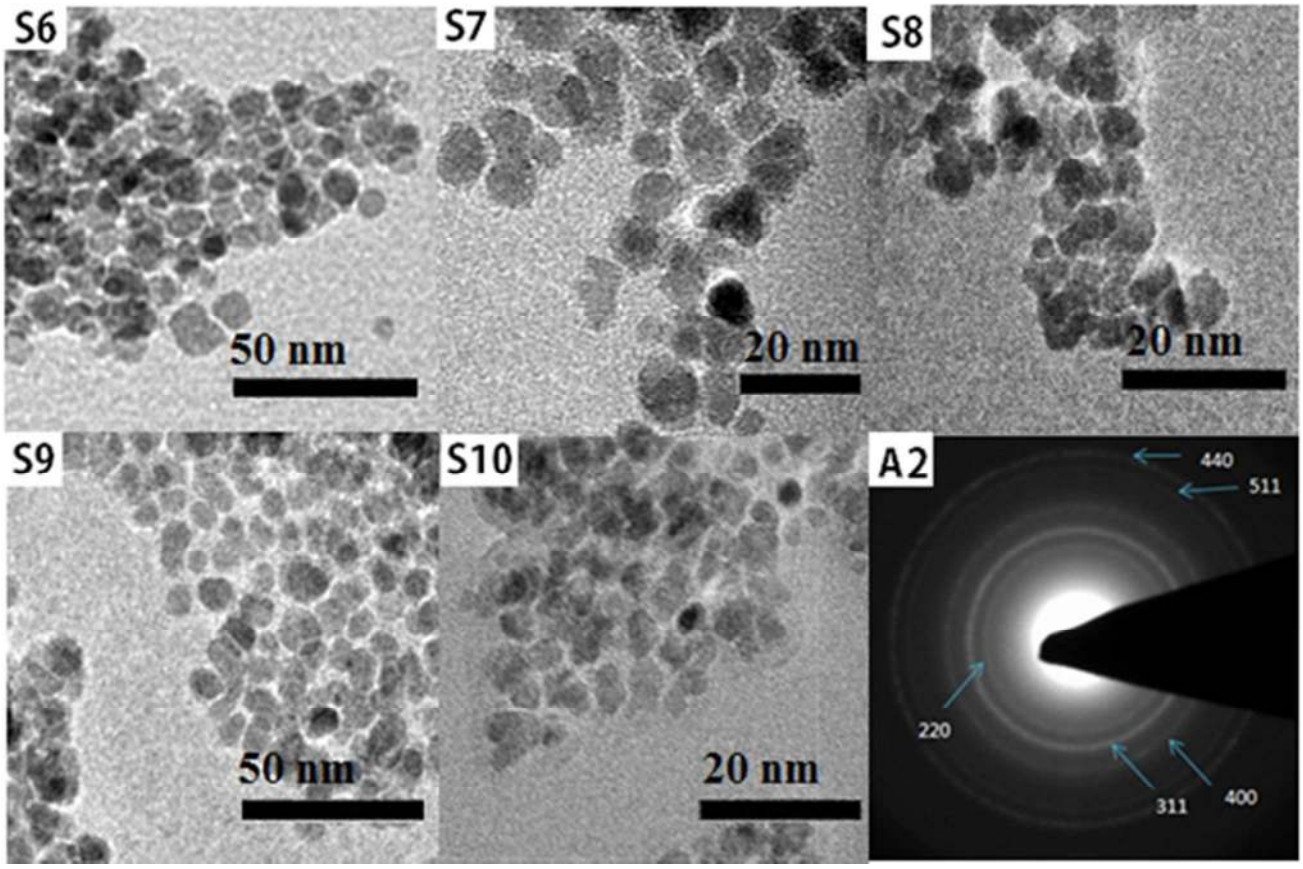

Fig. 2B. TEM images of the TA-SPIONs (S6), ATA-SPIONs (S7), TMA-SPIONs (S8), ATA-TA-SPIONs (S9), and ATA-TMA-SPIONs (S10) respectively, synthesized by the thermal decomposition method. A2 represents the SAED pattern of the ATA-TA-SPIONs (S9).

View Article Online
DOI: 10.1039/C6RA18567C

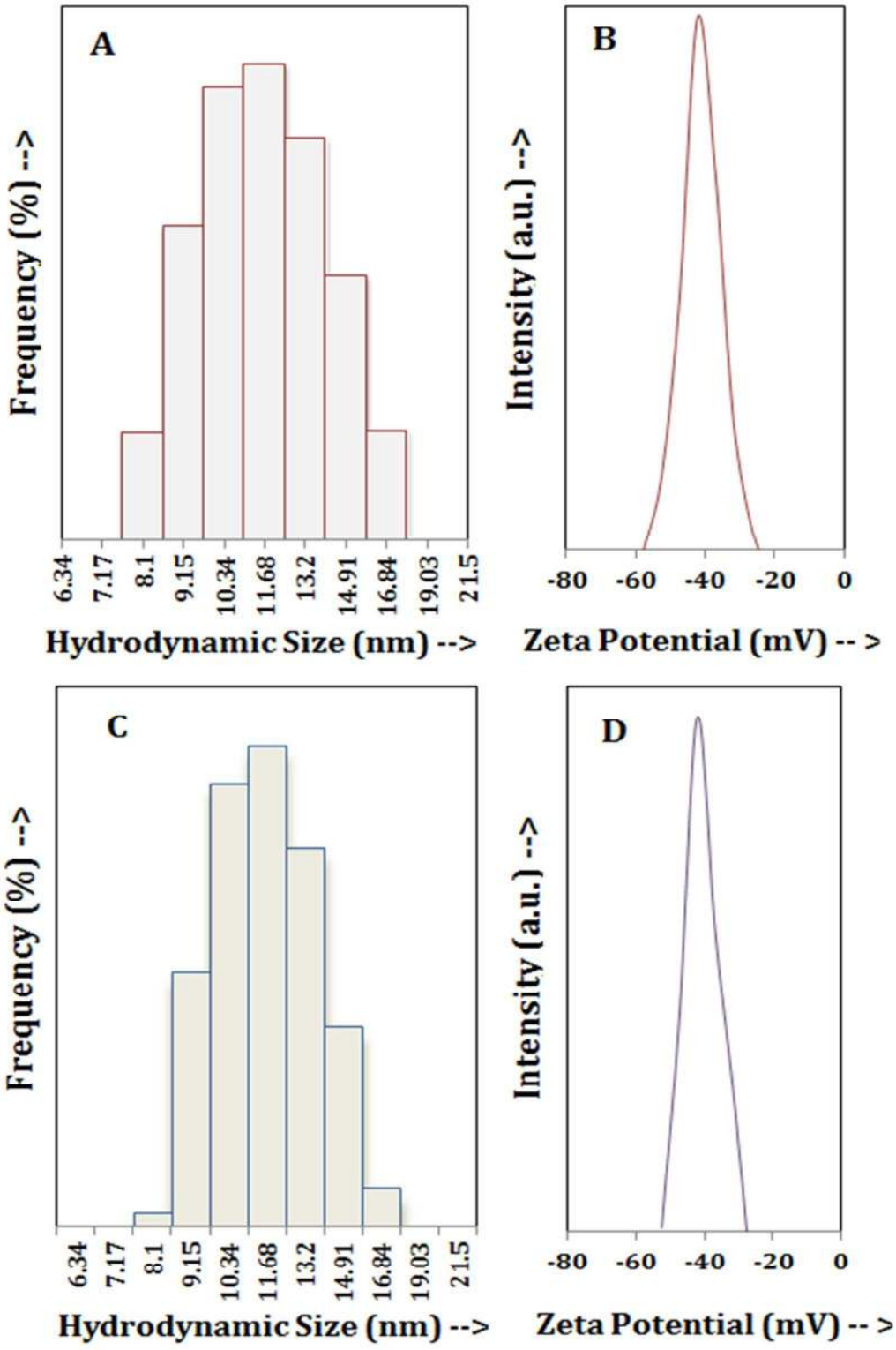

Fig. 3. (A & B). Hydrodynamic size & zeta potential of the TMA-SPIONs (S1). **(C & D)**. Hydrodynamic size & zeta potential of the TA-SPIONs (S6), respectively.

View Article Online
DOI: 10.1039/C6RA18567C

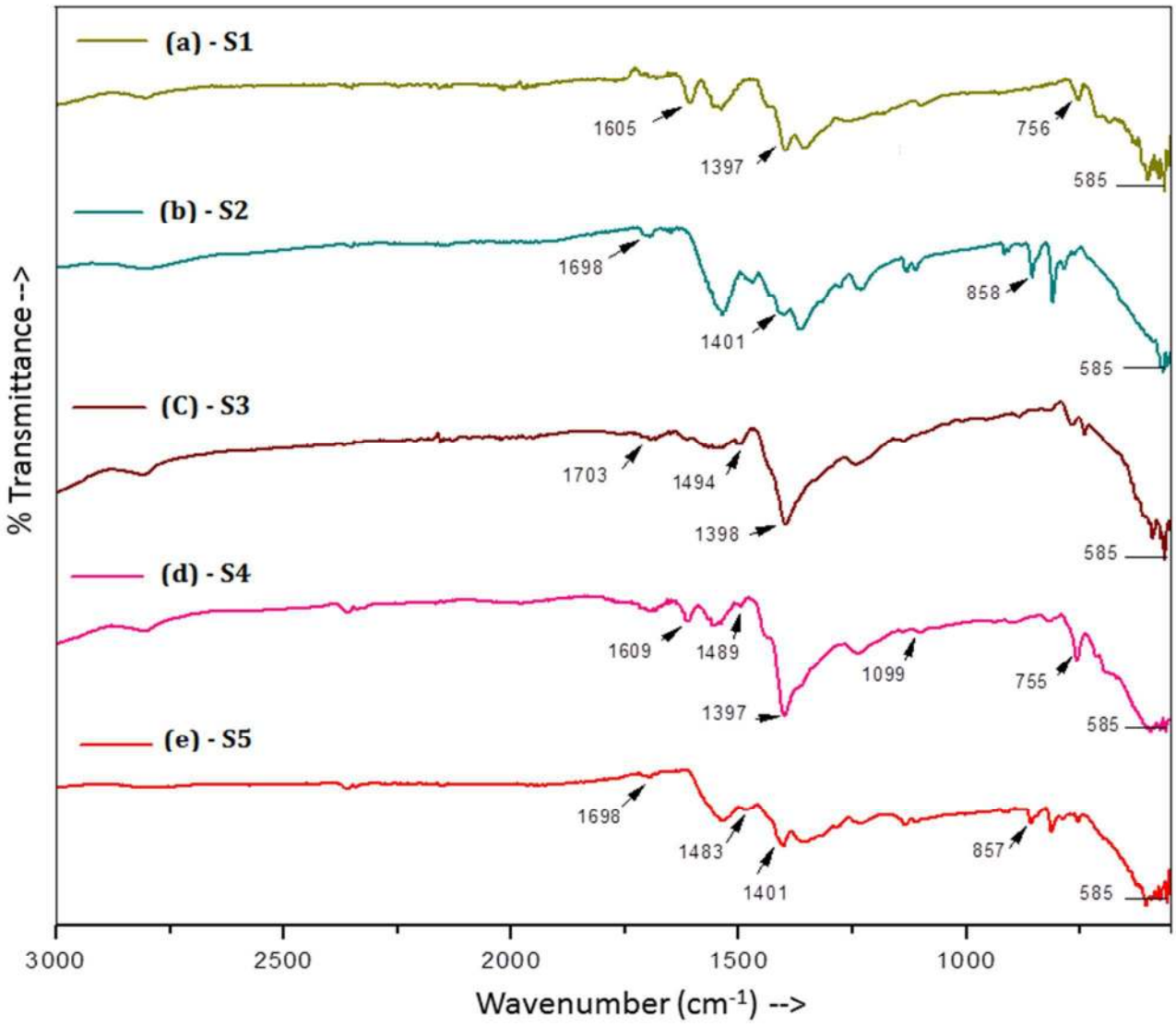

Fig. 4A. FTIR spectra of (a) TMA-SPIONs (S1), (b) PMA-SPIONs (S2), (c) ATA-TA-SPIONs (S3), (d) ATA-TMA-SPIONs (S4) and (e) ATA-PMA-SPIONs (S5), respectively, synthesized by the chemical co-precipitation method.

View Article Online
DOI: 10.1039/C6RA18567C

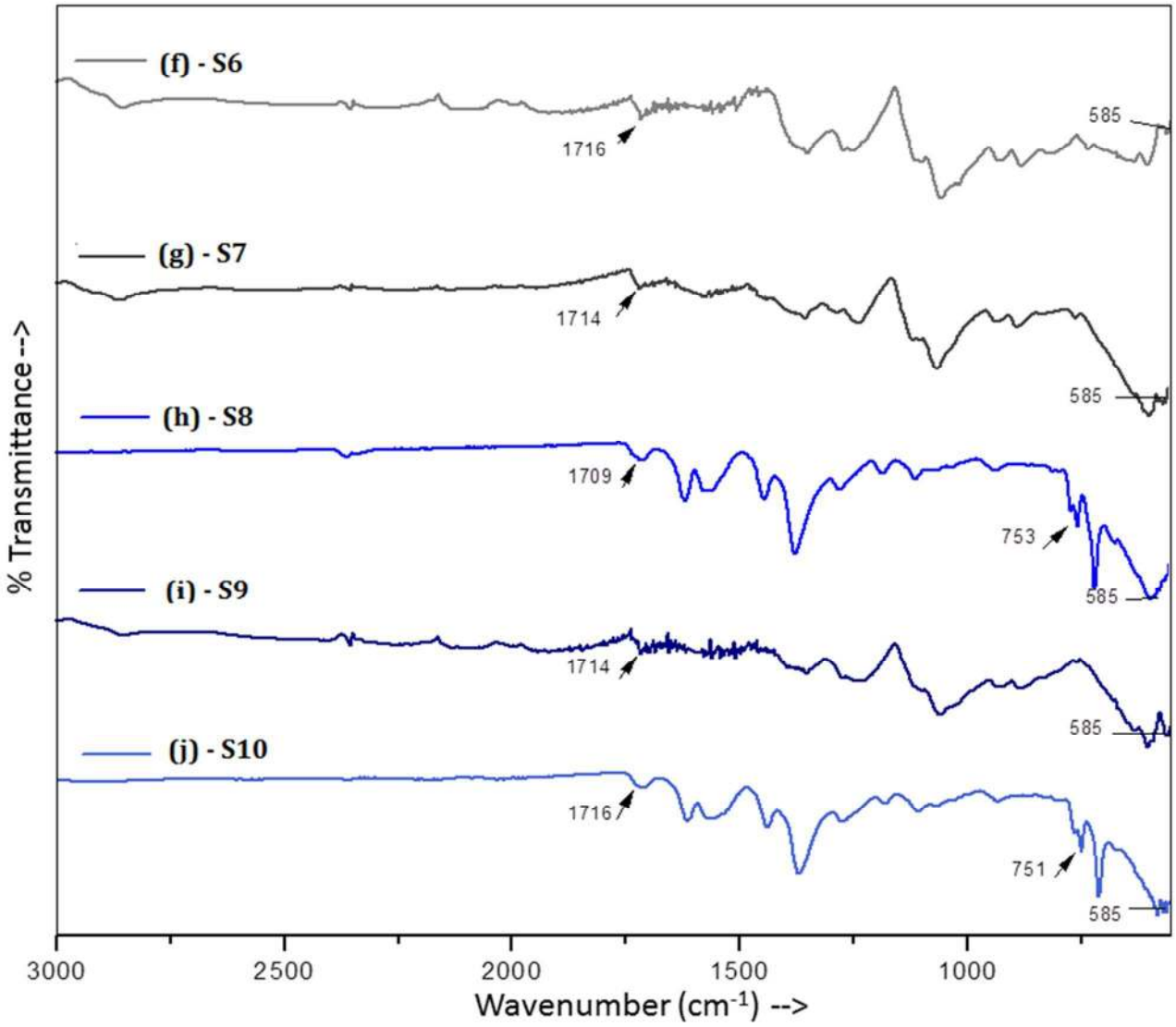

Fig. 4B. FTIR spectra of (f) TA-SPIONs (S6), (g) ATA-SPIONs (S7), (h) TMA-SPIONs (S8) (i) ATA-TA-SPIONs (S9), and (j) ATA-TMA-SPIONs (S10), respectively, synthesized by the thermal decomposition method.

View Article Online
DOI: 10.1039/C6RA18567C

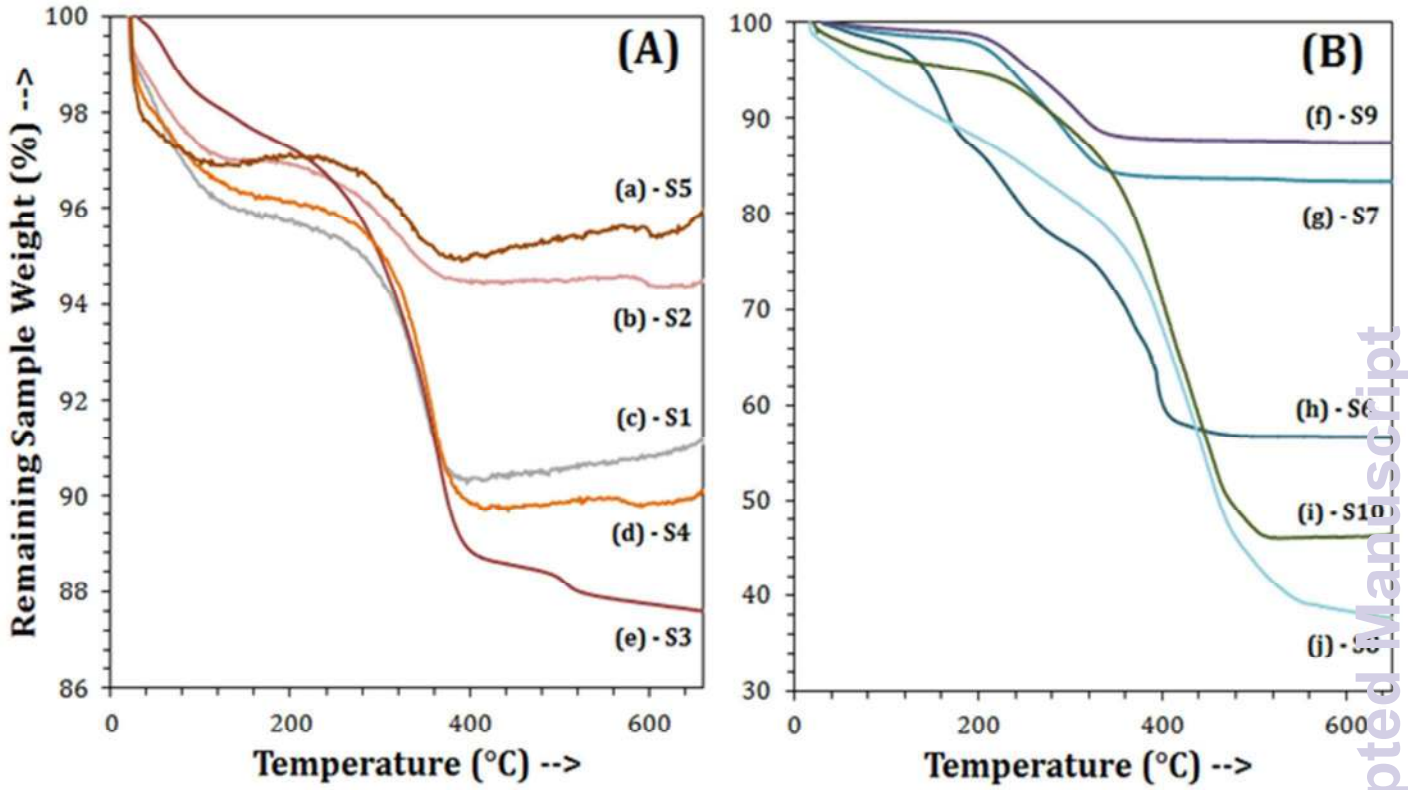

Fig. 5. (A) - TGA curves of the as-synthesized samples: (a) ATA-PMA-SPIONs (S5), (b) PMA-SPIONs (S2), (c) TMA-SPIONs (S1), (d) ATA-TMA-SPIONs (S4), and (e) TA-ATA-SPIONs (S3) respectively, synthesized by the chemical co-precipitation method. (**B) -** TGA curves of the as-synthesized samples of (f) ATA-TA-SPIONs (S9), (g) ATA-SPIONs (S7), (h) TA-SPIONs (S6), (i) ATA-TMA-SPIONs (S10) and (j) TMA-SPIONs (S8) respectively, synthesized by the thermal decomposition method.

View Article Online
DOI: 10.1039/C6RA18567C

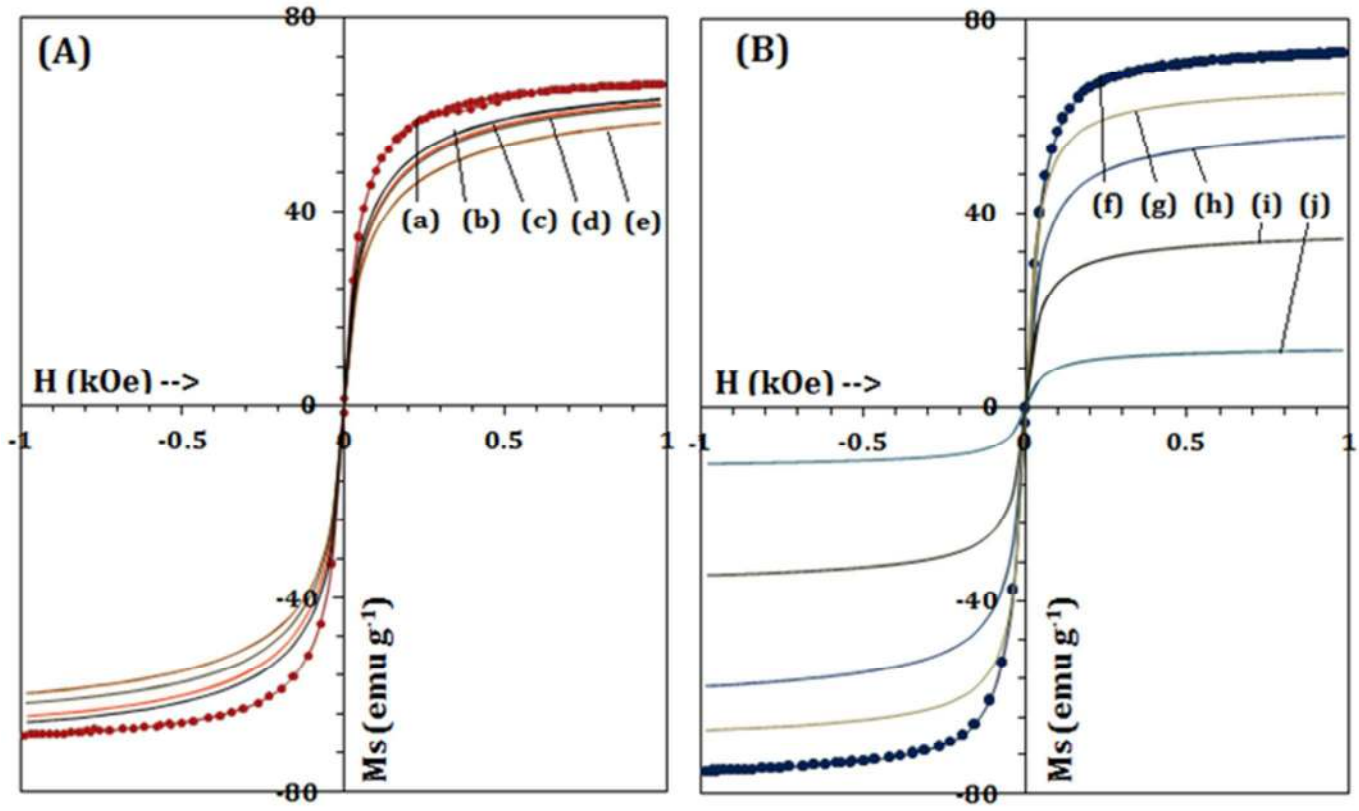

Fig. 6. (A) - Room temperature M–H curves of samples: (a) ATA-TA-SPIONs (S3), (b) ATA-PMA-SPIONs (S5), (c) PMA-SPIONs (S2), (d) ATA-TMA-SPIONs (S4) and (e) TMA-SPIONs (S1) respectively synthesized by the chemical co-precipitation method. (**B) -** Room temperature M–H curves of samples: (f) TA-SPIONs (S6), (g) ATA-TA-SPIONs (S9), (h) ATA-SPIONs (S7), (i) ATA-TMA-SPIONs (S10) and (j) TMA-SPIONs (S8) respectively synthesized by the thermal decomposition method. The M–H curves having maximum saturation magnetization values in both A and B are highlighted with the dots in the graph line.

View Article Online
DOI: 10.1039/C6RA18567C

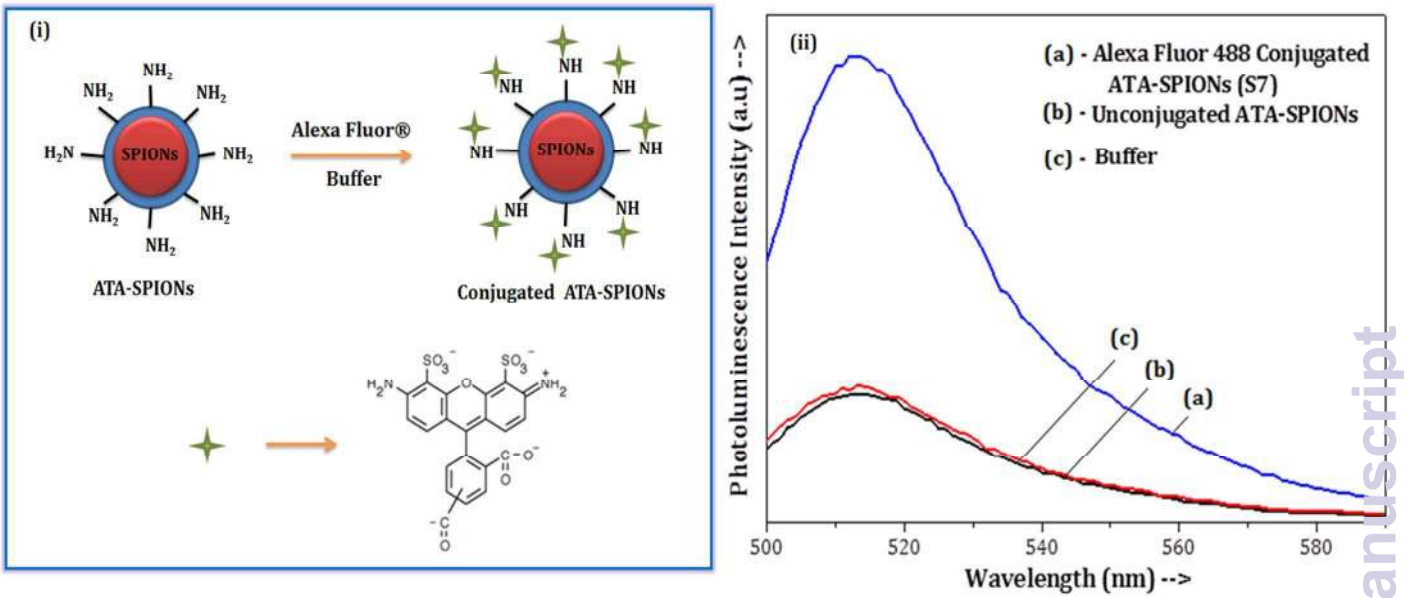

Fig. 7. (i) - Schematic diagram of the reaction mechanism in the conjugation of Alexa Flour 488 with ATA-coated SPIONs (S7) and **(ii)** - PL Spectra of (a) Alexa Flour 488 conjugated ATA-coated SPIONs (S7), (b) unconjugated ATA-SPIONs and (c) only buffer solution.

View Article Online
DOI: 10.1039/C6RA18567C

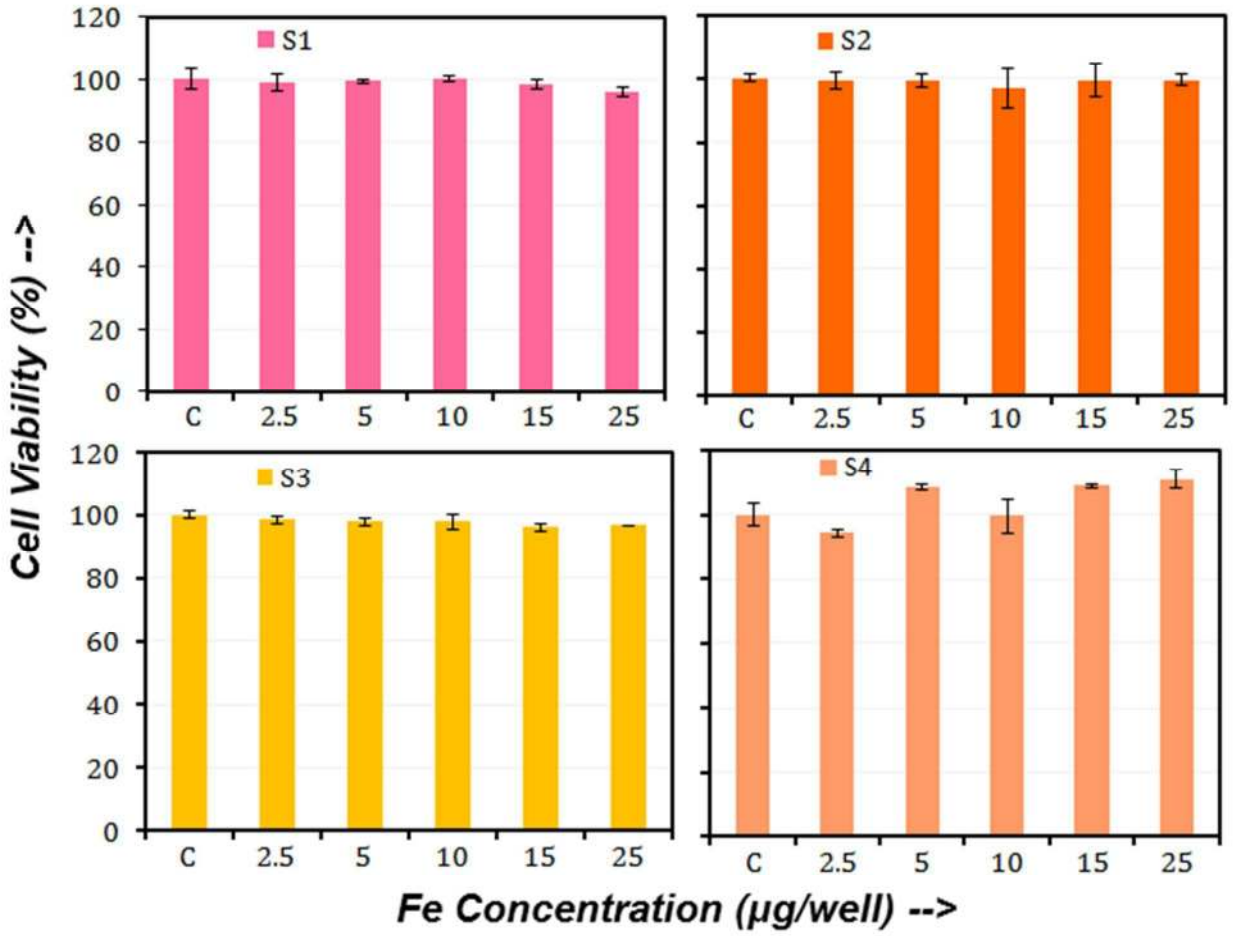

Fig. 8A. Cytotoxicity of samples (S1-S4) at different concentrations (2.5 – 25 µgFe/well) measured by trypan blue assay after 24 h incubation with MCF-7 breast cancer cells. Label C indicates the control wells (i.e., no SPIONs added).

View Article Online
DOI: 10.1039/C6RA18567C

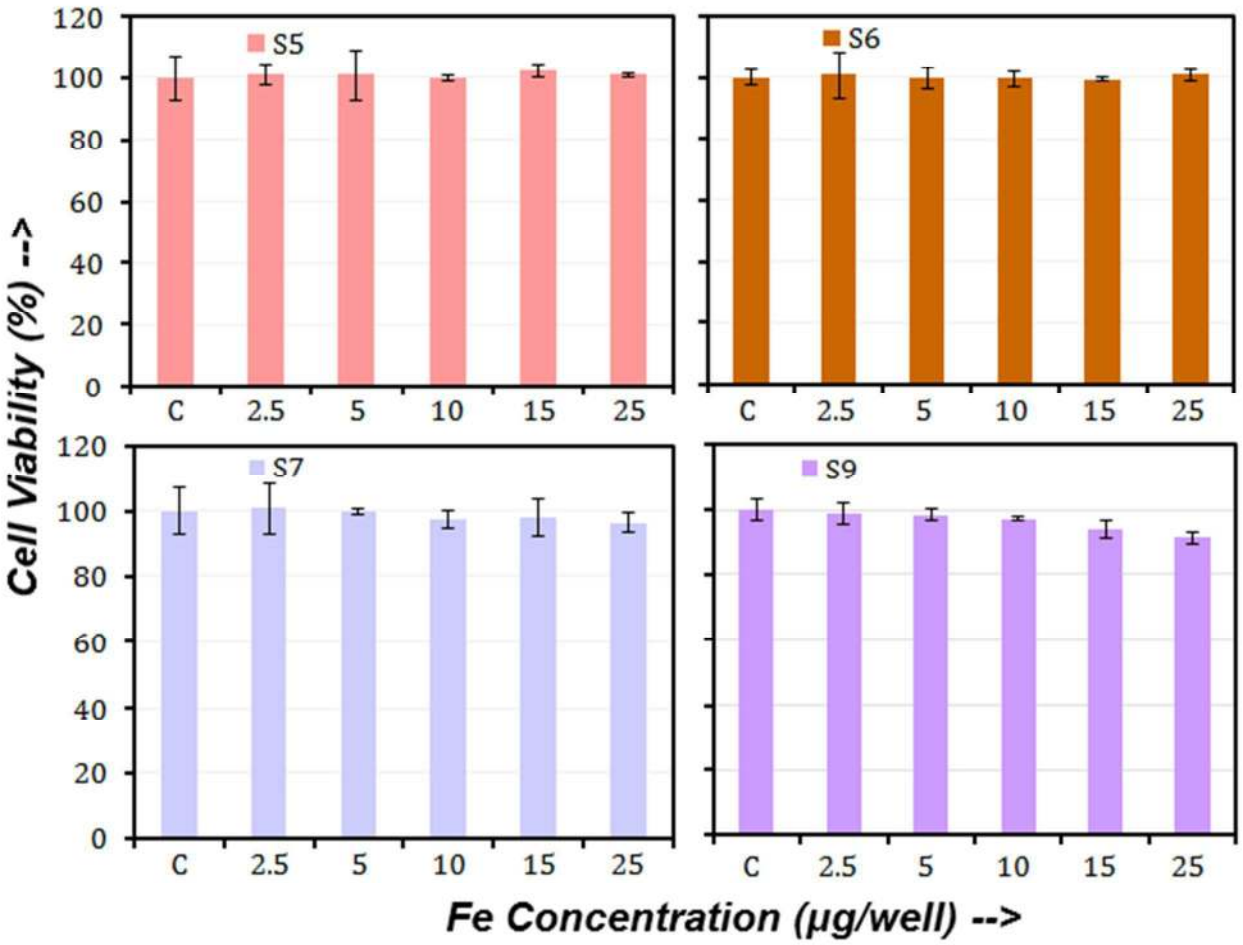

Fig. 8B. Cytotoxicity of samples (S5-S7 and S9) at different concentrations (2.5 – 25 µgFe/well) measured by trypan blue assay after 24 h incubation with MCF-7 breast cancer cells. Label C indicates the control wells (i.e., no SPIONs added).

View Article Online
DOI: 10.1039/C6RA18567C

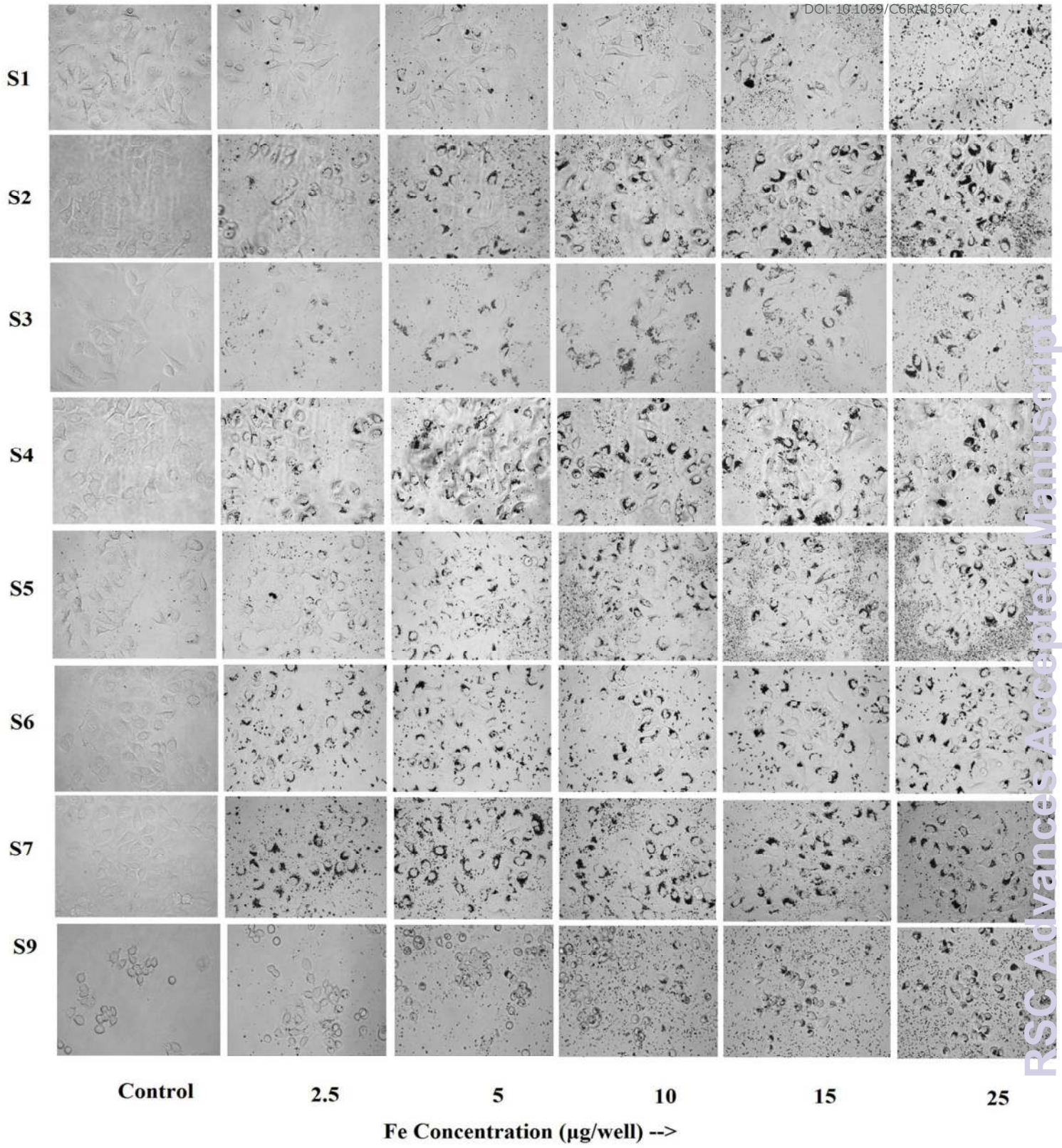

Fig. 9. Microscopic images of MCF-7 cancer cells after 24 h incubation with the samples of SPIONs (S1-S7 and S9) at concentrations ranging from 2.5 – 25 μg_{Fe}/well. Label C indicates the images of control wells (i.e., no SPIONs added) for respective concentrations. All microscopic images are taken at 400x magnification.

View Article Online
DOI: 10.1039/C6RA18567C

Novelty:

We report one-step facile synthesis of novel water-soluble and functionalized SPIONs, which could be promising candidates for cancer theranostics.

Graphical Abstract: